Geophysical Research Letters

RESEARCH LETTER
10.1029/2024GL109280

Potential Ozone Depletion From Satellite Demise During Atmospheric Reentry in the Era of Mega-Constellations

José P. Ferreira[1], **Ziyu Huang**[1], **Ken-ichi Nomura**[2], **and Joseph Wang**[1]

[1]Department of Astronautical Engineering, University of Southern California, Los Angeles, CA, USA, [2]Department of Chemical Engineering and Materials Science, University of Southern California, Los Angeles, CA, USA

Key Points:

- We present the first atomic-scale molecular dynamics simulation of high-temperature aluminum ablation during reentry from low-Earth orbit
- The amount of aluminum oxide nanoparticles generated is quantified and the accumulation in the atmosphere is estimated
- The long-term accumulation of aluminum oxides from reentering satellites can cause significant ozone depletion

Correspondence to:
J. Wang,
josephjw@usc.edu

Citation:
Ferreira, J. P., Huang, Z., Nomura, K.-i., & Wang, J. (2024). Potential ozone depletion from satellite demise during atmospheric reentry in the era of mega-constellations. *Geophysical Research Letters*, *51*, e2024GL109280. https://doi.org/10.1029/2024GL109280

Received 16 MAR 2024
Accepted 4 MAY 2024

Author Contributions:
Conceptualization: José P. Ferreira, Joseph Wang
Data curation: José P. Ferreira
Formal analysis: José P. Ferreira, Joseph Wang
Investigation: José P. Ferreira, Ziyu Huang, Ken-ichi Nomura, Joseph Wang
Methodology: José P. Ferreira, Joseph Wang
Project administration: Joseph Wang
Software: José P. Ferreira, Ziyu Huang, Ken-ichi Nomura
Supervision: Joseph Wang
Validation: José P. Ferreira, Joseph Wang
Visualization: José P. Ferreira
Writing – original draft: José P. Ferreira, Joseph Wang
Writing – review & editing: Joseph Wang

Abstract Large constellations of small satellites will significantly increase the number of objects orbiting the Earth. Satellites burn up at the end of service life during reentry, generating aluminum oxides as the main byproduct. These are known catalysts for chlorine activation that depletes ozone in the stratosphere. We present the first atomic-scale molecular dynamics simulation study to resolve the oxidation process of the satellite's aluminum structure during mesospheric reentry, and investigate the ozone depletion potential from aluminum oxides. We find that the demise of a typical 250-kg satellite can generate around 30 kg of aluminum oxide nanoparticles, which may endure for decades in the atmosphere. Aluminum oxide compounds generated by the entire population of satellites reentering the atmosphere in 2022 are estimated at around 17 metric tons. Reentry scenarios involving mega-constellations point to over 360 metric tons of aluminum oxide compounds per year, which can lead to significant ozone depletion.

Plain Language Summary With ongoing plans for many constellations of small satellites, the number of objects orbiting the Earth is expected to continue increasing in the foreseeable future. At the end of service life, satellites are disposed into the atmosphere, burning up during the process and generating aluminum oxides, which are known to accelerate ozone depletion. The environmental impacts from the reentry of satellites are currently poorly understood. This paper investigates the oxidation process of the satellite's aluminum content during atmospheric reentry utilizing atomic-scale molecular dynamics simulations. We find that the population of reentering satellites in 2022 caused a 29.5% increase of aluminum in the atmosphere above the natural level, resulting in around 17 metric tons of aluminum oxides injected into the mesosphere. The byproducts generated by the reentry of satellites in a future scenario where mega-constellations come to fruition can reach over 360 metric tons per year. As aluminum oxide nanoparticles may remain in the atmosphere for decades, they can cause significant ozone depletion.

1. Introduction

The ongoing development of extensive in-space infrastructures, such as satellite constellations, is expected to triple the count of tracked objects in low-Earth orbit (LEO) over the next century (ESA, 2023). The increasing number of satellites and launch vehicles remaining in Earth's orbit leads to an ever-growing need for post-mission disposal. International guidelines recommend that reentry occurs up to 25 years after mission termination (IADC, 2021), while the Federal Communications Commission (FCC) currently enforces a 5-year decommissioning obligation to limit orbital cluttering (FCC, 2022b). Concerns have been raised over the potential environmental impacts caused by the large number of reentering objects from LEO (FCC, 2021; FCC, 2022a).

Spacecraft burn up during atmospheric reentry, loosing an average of 51%–95% of their mass in the process (Anselmo & Pardini, 2005; Pardini & Anselmo, 2019). Aluminum is one of the most prevailing materials in satellites and launch vehicles by mass. Aluminum reacts with oxygen upon reentry in the atmosphere, generating aluminum oxides (Plane et al., 2021). Aluminum oxides have been recognized as a potential pollutant because they can interfere with stratospheric ozone chemistry. The chlorine activation reaction is catalyzed on the surface of aluminum oxide particles, with a reaction probability of 2% that boosts ozone depletion (Hanning-Lee et al., 1996; Molina et al., 1997).

In situ measurements showed evidence of a 1,000% increase in stratospheric aluminum levels from 1976 to 1984 (Zolensky et al., 1989), which was associated with the emission of hundreds of tons of such particles from solid rocket motors (SRM) during atmospheric ascent (Brady et al., 1994). Few observation campaigns have been carried out for vehicles reentering from LEO, and none covered the reentry of satellites. The cargo resupply

vehicle ATV-1 was studied during its mesospheric reentry using remote sensing through spectroscopy. Several instruments resolved spectroscopy peaks at 395 nm, which corresponds to aluminum (Lips et al., 2010), and in the 460–520 nm range, corresponding to aluminum oxide (Winter, 2014), right before the main explosion and breakup. A later study covering the reentry of the Cygnus OA6 spacecraft detected the presence of aluminum oxide at the same wavelength band after ablation in the mesosphere (Löhle et al., 2017). On-ground experimental studies were carried out to develop reentry breakup models for components made out of aluminum alloys (Beck et al., 2019; Bonvoisin et al., 2023). While these studies were able to replicate some byproducts of reentry and identify them through spectroscopy, they were not able to quantify the amount and resolve the size of such byproducts.

Potential environmental impacts were first assessed for SRM and focused on the direct injection of pollutants during the phase of ascent. Ross, Ballenthin, et al. (1997) addressed the short-term ozone depletion from chlorine directly exhausted by SRM. In situ measurements showed that nominal levels were recovered in about one hour after launch (Ross, Benbrook, et al., 1997), but the long-term impacts driven by aluminum oxides created in SRM exhaust plumes were not investigated. The contribution of aluminum from reentering satellites to ozone depletion was deemed to be negligible based on spacecraft reentry data from the 1990s although it was also acknowledged that larger deposition rates can have a significant impact in the ozone column density (Lohn et al., 1994). The aluminum oxidation process was studied for the ablation of meteors (Hunten et al., 1980; Plane et al., 2021), which have a much lower aluminum mass fraction and higher relative speed than anthropogenic objects reentering from LEO. Recently, Murphy et al. (2023) deployed a similar method to that of Ross, Ballenthin, et al. (1997) and found aluminum particles and other compounds of anthropogenic origin in stratospheric aerosols. The authors concluded that the mass from spacecraft reentry compounds exceeded that of cosmic dust, and that about 10% of large stratospheric sulfuric acid particles contain aluminum or other elements from spacecraft reentry.

One notes that the number of tracked human-made objects in the mid 1990s was estimated to be 7,000—around 20% of today's (ESA, 2023). In 2022, the total mass of reentering objects was estimated to be 332.5 metric tons (ESA, 2023), a 21% increase from the previous year, with 93% of that mass originated from LEO. More than one million radio-frequency spectrum allocation requests were made for planned satellites over the last 5 years (Falle et al., 2023). Forecasts point to future reentry rates of 800–3,200 metric tons per year for satellites, and up to 1,000 metric tons per year for launch vehicles (Organski et al., 2020). The engineering approach of design-for-demise (Kärräng et al., 2019; Waswa & Hoffman, 2012) and the deployment of active debris removal solutions may further exacerbate the aforementioned trend. As for natural sources, meteoroids enter the atmosphere at an average rate of over 11,750 metric tons per year (Drolshagen et al., 2017).

In view of the aforementioned forecasts, several modeling studies have been carried out to estimate environmental impacts of spacecraft demise in the atmosphere. Bekki et al. (2021) carried out computational fluid dynamics modeling for non-equilibrium chemically reacting flows (Scott et al., 2004) and concluded that nitrogen oxides and chlorine are expected to be created upon reentry and long-term ozone depletion is expected to be located over Antarctica at high altitudes. Bianchi et al. (2021) used the Gibbs energy minimization procedure (Park et al., 2021) to estimate the non-equilibrium generation of aluminum and titanium oxides. Both studies started from an average satellite composition and reentry scenarios to infer the mass fraction lost as a function of altitude. However, the size of particles emitted to the atmosphere was not resolved and the byproducts were not clearly quantified, preventing a clear understanding of the long-term impacts driven by aluminum oxides generated from reentering satellites. It is theorized that the planned increase in LEO satellites can contaminate up to half of stratospheric sulfuric acid particles with metals from reentry (Murphy et al., 2023).

This paper studies the demise process of satellites through thermal ablation during atmospheric reentry and the accumulation of aluminum oxides in the mesosphere. The focus is on potential environmental impacts such as ozone depletion. We present, to our knowledge, the first atomic-scale molecular dynamics (MD) simulation study of the relevant aluminum oxidation process. This method resolves the reaction byproducts, quantifies the aluminum oxide yield, and determines the size distribution of the resulting particles. The MD simulation results are then extrapolated to estimate the long-term accumulation of aluminum oxides in the atmosphere which can potentially interfere with stratospheric ozone.

2. Methodology

2.1. Approach

We consider a generic satellite reentering the mesosphere from LEO. The satellite structure is taken to be entirely aluminum, and the relevant ambient gas is molecular oxygen (COESA, 1976; Plane et al., 2021). In this study, we first carry out an atomic-scale MD simulation—a first-principle informed method for modeling physical and chemical interactions between atomic particles (Rahman, 1964)—to simulate the bond breakage between aluminum atoms (Al-Al bonds) due to the impact of oxygen molecules (O-O bonds) and the formation of aluminum oxides (Al-O bonds) during the ablation stage of reentry. The byproducts generated during the oxidation process are defined as clusters of aluminum oxides (AlO cluster) and aluminum (Al clusters). We then extrapolate the mass of byproducts for the entire population of satellites reentering from LEO from 2016 to 2022 (ESA, 2017; ESA, 2023) and estimate the clusters' gravitational settling time in the atmosphere. Finally, we present an estimation of the long-term accumulation of these byproducts in the mesosphere along with a comparison against natural levels.

MD simulations have been extensively used to model the oxidation process of metals, including aluminum (Li et al., 2013; Vashishta et al., 2006). An MD model utilizes empirical force fields to describe the behavior of a given set of atoms. This study applies the reactive force field (ReaxFF) to model chemical bond breakage and formation (Van Duin et al., 2001), and the RXMD framework (Nomura et al., 2020) recently developed for high-performance parallelized MD simulations. The ReaxFF MD model was previously applied to study hypervelocity impacts on aluminum (Zhang et al., 2008), silver and gold erosion by atomic oxygen in LEO (Morrissey et al., 2019), and water formation by meteoroid impacts on the Moon (Huang et al., 2021). The force fields used in this ReaxFF MD model were generated for an aluminum-oxygen system (Hong & van Duin, 2015):

$$E_{sys}\left(\{\vec{r}_{ij}\},\{\vec{r}_{ijk}\},\{q_i\}\right) = E_{bond} + E_{over} + E_{under} + E_{lp} + E_{val} + E_{tors} + E_{Waals} + E_{Coul} \quad (1)$$

where the total energy within the system (E_{sys}) is a function of the interatomic distance for a pair of atoms (r_{ij}), triplets (r_{ijk}), and the atomic charge (q_i). The valence interactions comprise the bond energy (E_{bond}), over-coordination (E_{over}), under-coordination (E_{under}), lone-pair (E_{lp}), valence angle (E_{val}), and torsion angle (E_{tors}) energy terms. The non-covalent interactions include the Van der Waals (E_{Waals}) and the Coulomb (E_{Coul}) energy terms. The explicit definition of each energy term can be found in Van Duin et al. (2001).

The MD simulation runs until the number of Al-O bonds stabilizes, and the output is used to determine the size of byproducts generated during reentry from LEO. To calculate the gravitational settling time of such clusters of particles in the atmosphere, an atmospheric model is deployed based on the U.S. Standard Atmosphere model (COESA, 1976). Here, the viscous force (F_v) is modeled according to Stokes' Law as a function of the atmospheric kinematic viscosity (μ), the cluster's aerodynamic diameter (d_a) and velocity (v), and the Cunningham correction factor (C_c):

$$\vec{F}_v = -\frac{3\pi\mu d_a}{C_c}\vec{v} \quad (2)$$

where

$$C_c = 1 + K_n\left(1.100 + 0.570e^{-1.144/K_n}\right) \quad (3)$$

is an empirical factor applied to Stokes' law which accounts for the effects of non-continuum flow impacting small particles (Cunningham, 1910). This allows resolving viscous forces until the mesopause (Davies, 1945; Knudsen & Weber, 1911). The Knudsen number ($K_n = 2\lambda/d_a$) compares the altitude-dependent mean free path (λ) and the aerodynamic diameter.

Assuming steady state conditions and no further mass loss after the thermal ablation stage emulated in the MD simulations, the gravitational force (F_g) on the cluster is defined in Equation 4. We take the aerodynamic diameter d_a to be the characteristic length of a unit density sphere ($\rho_0 = 1{,}000\ \mathrm{kg/m^3}$) that has the same shape and mass (m_c)

as the cluster. This provides the diameter of a water sphere with the same settling velocity as the cluster (Thomas & Charvet, 2017).

$$\vec{F}_g = m_c\vec{g} = \frac{\pi}{6}\rho_0 d_a^3\vec{g} \tag{4}$$

We then resolve the one-dimensional dynamics of the clusters by iteratively solving Equation 5. This provides the cluster velocity, which can then be used to retrieve the geometric altitude as a function of time. The initial altitude is the same as that of the reentry event, and we assume null initial velocity for byproducts of thermal ablation.

$$\vec{F}_g + \vec{F}_v = m_c\frac{d\vec{v}}{dt} \tag{5}$$

2.2. Simulation Setup

We consider a typical small satellite, representative of a mega-constellation node, with a total mass of 250 kg and volume of $3.2 \times 1.6 \times 0.2$ m^3. The typical range of structural mass fraction for satellites is 15%–40% (Schulz & Glassmeier, 2021; Wertz et al., 2011), with most structural elements made of aluminum alloys (SpaceX, 2020). We assume 30% of the total mass of the satellite to be made of aluminum (Bonvoisin et al., 2023). Past studies have shown that thermal ablation is the dominant method for energy transfer during atmospheric reentry for large bodies such as satellites. This is in contrast to sputtering (or *vaporization*) that prevails for low-mass and high-speed entering bodies such as micrometeoroids which demise before the temperature reaches 2,200 K (Ceplecha et al., 1998). Therefore, it is considered that sputtering plays a negligible role in the mass loss process for satellites (Guttormsen et al., 2020).

As the satellite reenters from LEO in a high-temperature process dominated by thermal ablation at 2,200 K, we consider a worst-case scenario: 90 s at constant attitude coinciding with the largest wetted area. The altitude is set at 86 km where the molecular oxygen number density is 3.0×10^{19} m^{-3} (COESA, 1976). Such a scenario is supported by previous observations of the ATV-1 reentry for duration, altitude, and maximum temperature (Lips et al., 2010, p. 3).

The MD simulation initial configuration is depicted in Figure 1a. MD simulations are carried out in a domain with periodic boundary conditions, comprising 960 to 1,360 aluminum atoms and 100 to 300 oxygen atoms. The aluminum crystal is structured in a face-centered cubic (*fcc*) lattice with the (111) surface exposed to the incoming oxygen molecules as it is the closest-packed, most stable configuration in an *fcc* crystal (Eberhart & Horner, 2010). The lattice constant for the aluminum structure is 0.404 nm (Jette & Foote, 1935).

In the simulation, the aluminum and oxygen samples are first heated from 100 K (Figure 1a) to 2,200 K. Then, molecular oxygen impinges onto the aluminum surface along the normal direction at 2 km/s. This endures for up to 144,000 time steps with a variable time step ranging from 0.01 to 0.25 fs in duration (Ferreira et al., 2023a). Such duration must be at least one order of magnitude lower than the highest vibrational frequency of each bond (Hong & van Duin, 2015)—criterion met in our case for the most restrictive condition of the molecular oxygen double bond (Huber & Herzberg, 2013). The averaged atomic position of the last time steps (Figure 1b) is used to group atoms into clusters made of solely aluminum (Al) or aluminum oxides (AlO). The mass m_c of each cluster is then defined by accounting for the atomic mass of each species, then used to compute the aerodynamic diameter d_a as depicted in Equation 4.

The simulation cases are summarized in Table 1a. Cases I to IV are validation cases, and are performed for a cross-sectional area of 2.2×1.9 nm^2. Case V is the extrapolation case, covering an area of 4.9×2.5 nm^2. The domain size in the normal direction is of 88 nm.

To scale up the MD simulation results, two similarity parameters are defined to ensure comparability between macro- and atomic-scale scenarios. The *molar ratio* is defined as the ratio between oxygen and aluminum, which is constant in both macro-scale ($R^m_{O/Al}$) and atomic-scale ($R^a_{O/Al}$) scenarios. As for the *scaling factor*, it is defined as the ratio between reactants of the same species in both scenarios for aluminum $\left(S_F^{Al}\right)$ and oxygen $\left(S_F^{O}\right)$, which is invariant for both species. The amount of macro-scale reactants can be computed by equating the aluminum mass fraction, and by accounting for the reentry duration, velocity, altitude, and wetted area for oxygen. Atomic-scale

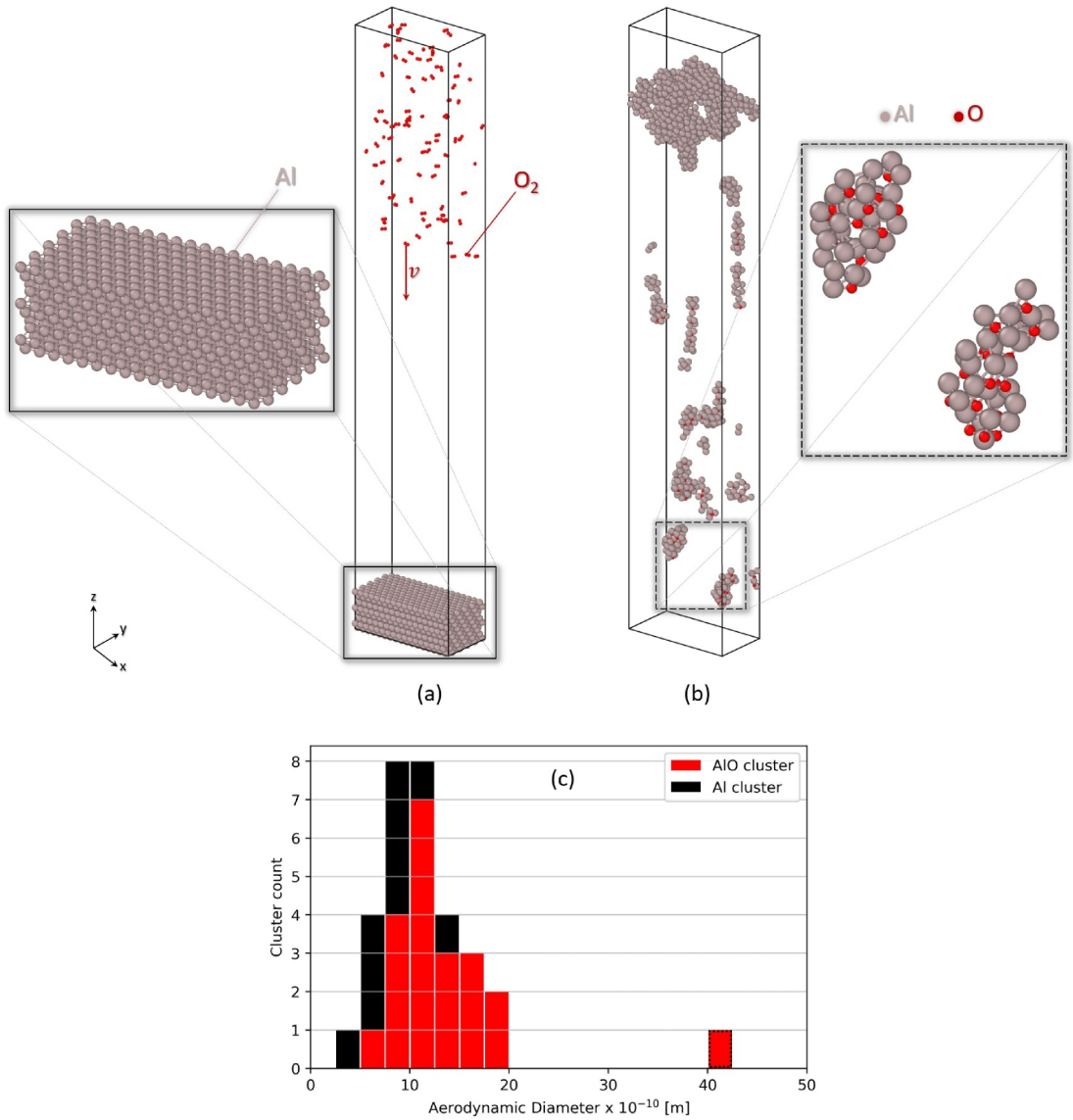

Figure 1. Snapshots from the simulation process of Case V at (a) $t = 0$ ps, and (b) $t = 28.7$ ps. The sample aluminum structure (gray atoms) is impinged by oxygen molecules (red atoms), with visualization sourced by OVITO (Stukowski, 2009). The atomic structure is depicted at the start of the heating process, at 100 K (a). The molecular structure is altered once the oxygen molecules impact into the aluminum slab with velocity v, at 2,200 K. By the end of the simulation, AlO clusters (red and gray atoms) and Al clusters (gray atoms) can be observed (b). The corresponding particle size distribution is exhibited in the histogram (c) for the aerodynamic diameter of AlO and Al clusters (red and black bars).

values are derived from the MD simulation and presented in Table 1a as N_O and N_{Al}. Therefore, the macro-scale molar ratio $R^m_{O/Al}$ is 0.130, and the scaling factor is approximately 10^{24} for both species (Ferreira et al., 2023b).

3. Results and Discussions

3.1. Validation

The consistency of the methodology is first validated for different molar ratios, where the initial number of oxygen atoms (N_O) and aluminum atoms (N_{Al}) varies in Cases I through IV (Table 1a). The impingement of molecular oxygen onto the aluminum structure causes the dissociation of the former and the formation of Al-O bonds (N_{Al-O}), equivalent to the snapshot of Figure 1b. Metrics for comparison are defined by the ratio of O-O bonds broken and Al-O bonds formed ($R_{O-O/Al-O}$), and results are shown in Figure 2a depicting the bond count as a function of time. Similar slope values during the impingement period denote equivalent chemical reaction rates,

Table 1
Atomic and Bond Count for Different Simulation Cases, With Steady-State Values Averaged for the Last 24,000 Time Steps of the Simulation

(a) Overall picture of initial and steady-state bond counts.

Case	N_O	N_{Al}	$R^a_{O/Al}$	N_{Al-O}	$R_{O-O/Al-O}$
I	100	1,024	0.0977	375	0.133
II	134	1,024	0.131	506	0.132
III	200	1,024	0.195	775	0.129
IV	300	960	0.313	1,185	0.127
V	176	1,360	0.129	654	0.135

(b) Detailed Al-O and O-Al bond count for steady state in Case V.

Bond pair	Index 0	Index 1	Index 2	Index 3	Index 4	Index 5
Al-O_a	924	250	157	26	3	0
O-Al_b	0	0	4	40	131	1

and the asymptote achieved toward the end of the simulation proves that steady state had been reached. Similar $R_{O-O/Al-O}$ values showcased in Table 1a support the scalability of the methodology.

Results also show that aluminum oxides formed during atmospheric reentry are on the verge of liquid state. An applicable validation tool lies on computing the pair distribution function (PDF) to map interatomic distances for Al-O and Al-Al bonds. As such, the molecular structure of the clusters (Figure 2b) is validated against literature where the PDF at 2,400 K for Al-O bonds peaks at 0.178 nm, and at 0.280 nm for Al-Al bonds (Skinner et al., 2013). This strongly agrees with results obtained for Cases I through IV at 2,200 K with a cutoff radius of 1 nm and 200 data bins as showcased in Figure 2b: the average position of each atom over the last 24,000 time steps is used to compute a partial PDF that peaks at 0.183 and 0.288 nm for Al-O and Al-Al bonds respectively.

3.2. Atomic-Scale Simulation

Having validated the compatibility of our MD simulations with experimental results for molten aluminum oxide, we now focus on Case V where the atomic-scale molar ratio $R^a_{O/Al}$ approximates that of macro scale. We also observed similar reaction rates in Cases I through IV where the thickness of the aluminum core varied. Case V presents a higher thickness while approaching the width-to-length ratio of the satellite.

The number of Al-O bonds shown in Figure 2a is defined as the summation of individual bonds between aluminum and oxygen atoms, meaning that the number of O-Al bonds would be reciprocal. However, to resolve byproducts from the oxidation reaction, one needs to account for the central atom of each pair and quantify the number of bonds established. Here, the number of Al-O bonds is broken down into bond pairs of Al-O_a and O-Al_b, where $a,b \in \mathbb{N}$. This allows quantifying the aluminum atoms partaking in AlO and Al clusters, that is, the byproducts observed in Figure 1b.

At steady state, the position of each atom is retrieved and clusters of AlO and Al are defined, resulting in 31 conglomerates ranging from a massive AlO cluster of 831 atoms to a single, monoatomic Al cluster. The detailed bond count analysis of Case V is summarized in Table 1b. All non-zero a and b indices present the atomic count for central atoms partaking in AlO clusters, whereas the remaining zero index accounts for the atoms not involved in the oxidation reaction. This allows concluding that 436 aluminum atoms and 176 oxygen atoms constitute different AlO clusters, whereas Al clusters are comprised of 924 aluminum atoms. It is worth noting that all oxygen is consumed in the oxidation reaction as suggested by the decreasing number of O-O bonds in Figure 2a and confirmed by the null O-Al_b bond count for $b = 0$. Moreover, the surplus of aluminum atoms leads to the creation of several Al clusters, confirming that this reaction occurs in an oxygen-deficient environment as previously suggested by the low molar ratio.

The mass m_c of each cluster is then computed by accounting for the atomic count and mass of each chemical species depicted in Table 1b. This allows retrieving the aerodynamic diameter d_a as per Equation 4 for both clusters, presented in the histogram of Figure 1c. Aluminum clusters are smaller in size due to the direct high-energy impingement of oxygen molecules into the aluminum surface, while AlO clusters grow larger as they derive from the oxidation reaction. Note that the dash-contoured AlO cluster found at the upper end of the aerodynamic diameter range in Figure 1c is mostly made out of aluminum, although containing few oxygen atoms enclosed. It is the result of the aforementioned oxygen-deficient reaction, being the remnant of the thermal ablation process. This large cluster can be spotted in the upper portion of Figure 1b.

Based on the cluster size distribution, an estimation of the gravitational settling time for such particles is carried out by resorting to the balance of gravitational and viscous forces as per Equation 5. The aerodynamic diameter is used as the characteristic length for viscous force calculations. The variable of interest is the residence time in the atmosphere before triggering putative ozone-depleting reactions. Data show that 90% of Earth's ozone is located in the stratosphere, with concentrations peaking between 20 and 30 km of altitude in spite of seasonal and geographical variations (Weidmann, 2021). During the Montreal Protocol era, most of the ozone depletion due to

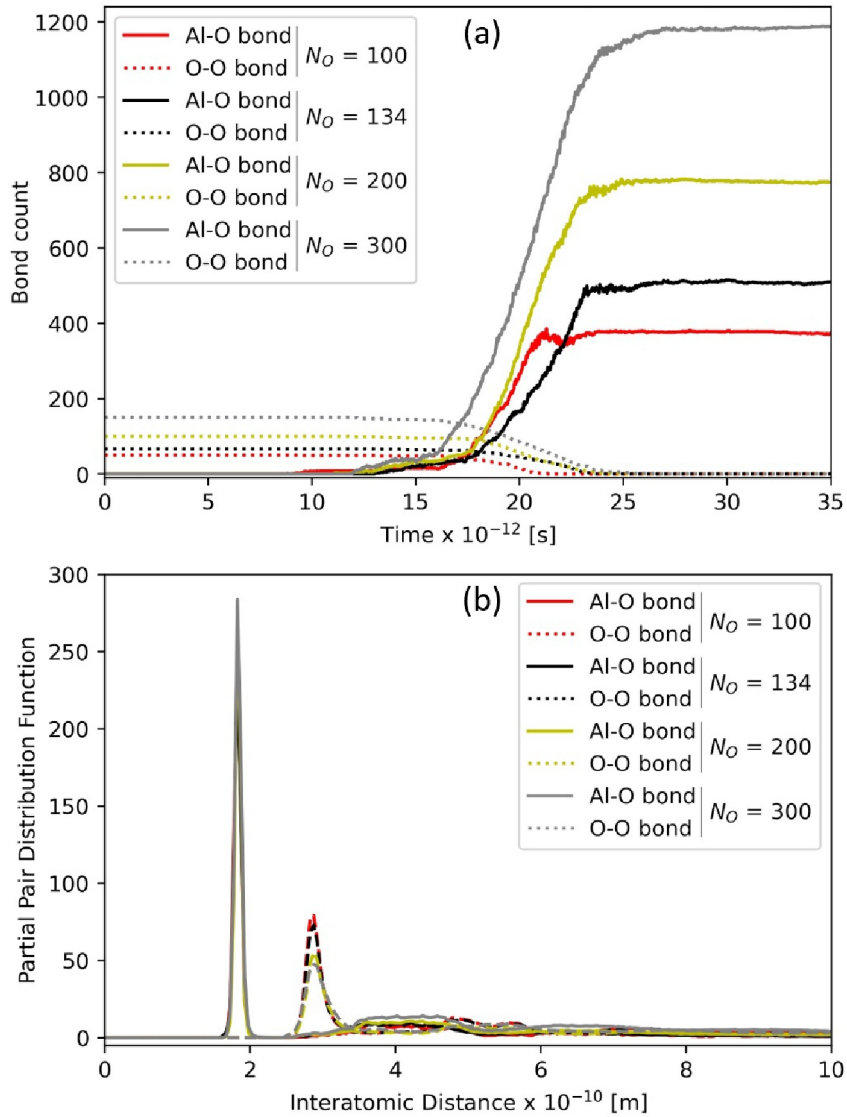

Figure 2. Results for Cases I through IV. (a) Time history for the O-O bond breakage and Al-O bond formation. (b) Partial pair distribution function for aluminum oxides at 2,200 K resulting from the reentry scenario.

anthropogenic chlorine took place at 15 and 40 km, at an average rate of −7.3% per decade (Randel et al., 1999). Therefore, given that aluminum oxides catalyze chlorine activation, the cluster settling time is defined as the shortest period between the byproduct generation in the mesosphere and the closest altitude of concern, at 40 km.

The differential equation is iteratively solved for a null initial velocity at a geometric altitude of 86 km. The settling time is computed for clusters such as the ones presented in Figure 1c, with aerodynamic diameter ranging within 0.4–4.2 nm. At macro scale, the expected value for the aerodynamic diameter is estimated to be 4.1 nm (Ferreira et al., 2023b), taking up to 30 years to reach the altitude of 40 km.

We emphasize that all clusters presented are classified as nanoparticles. At this length scale, particles are known to be dominated by nucleation processes and tend to condense with one another to grow into larger clusters. Although coagulation is a widely studied tropospheric process wherein nanoparticles have a relatively short existence and rapidly grow into larger clusters, its effects in the mesosphere are poorly understood. Additionally, the dynamics of nanoparticles within the homosphere is highly influenced by diffusion through turbulent mixing and Brownian motion. Previous studies suggested that turbulence-induced diffusion is efficient for clusters in the 90–95 km altitude range (Hunten et al., 1980) but negligible below 80 km. Although our results match those from

Lohn et al. (1994) for stratospheric settling of reentry byproducts, further three-dimensional atmospheric modeling is recommended to resolve both vertical and quasi-horizontal dynamics.

3.3. Full-Scale and Long-Term Extrapolation

We next extrapolate the results of the atomic-scale simulations to the macroscopic scenario using the similarity parameters for a small satellite. As the molar ratio between reactants in atomic- and macro-scale scenarios ensures interchangeability, one may infer the macro-scale byproduct's mass by equating the scaling factor in the mass of AlO and Al clusters retrieved from MD simulations. Such is achieved by accounting for the atomic count of aluminum and oxygen atoms in AlO clusters, and aluminum atoms in Al clusters available in Table 1b.

It is then possible to infer that a single reentry event of a 250-kg satellite with a 30% aluminum mass fraction yields approximately 29.8 kg worth of AlO particles and 51.0 kg of Al after thermal ablation, in the higher mesosphere. Solely 24.0 kg of the initial aluminum mass is oxidized into AlO particles, leading to a 68% mass fraction of non-oxidized aluminum. This can be interpreted as the remnant of the satellite structure that does not get oxidized during the thermal ablation stage of reentry, which is consistent with the aluminum-rich AlO cluster of Figure 1c acknowledged in the previous section as a consequence of the oxygen-deficient oxidation reaction. Conversely, the remaining clusters in that same histogram are interpreted as the byproducts of thermal ablation during atmospheric reentry. One should note that surface oxidation will occur as aluminum-rich conglomerates settle in the atmosphere.

To extrapolate the one-satellite results to the entire population of reentering satellites, data from the yearly ESA's Annual Space Environment Report are used since its first issue (ESA, 2017; ESA, 2023). As LEO spacecraft make up for the majority of reentering objects and the atomic-scale simulation was carried out for conditions of LEO reentry, we only utilize reentry data related to LEO spacecraft for this extrapolation. Note that each yearly report summarizes the reentry activity from the previous year, ranging from 2016 to 2022, and that reentered satellite-related data cover the categories defined in the reports as *Payload*, *Payload Fragmentation Debris*, *Payload Debris*, and *Payload Mission Related Object*. Moreover, a *future mega-constellations scenario* is also included to provide an estimation of forthcoming reentries accounting for mega-constellations (Organski et al., 2020).

In this long-term assessment, we first analyze the mass fraction of aluminum at the top of the atmosphere (TOA)—that is, before thermal ablation—and compare anthropogenic against natural sources. For satellite-related objects, a 30% mass fraction of aluminum is used, in line with the atomic-scale simulation assumptions. The contribution of natural sources to the overall TOA aluminum can be assessed by analyzing the micrometeoroid flux density. Both are compared through the *excess ratio*, defined as the ratio of aluminum mass of anthropogenic to natural sources.

Studies have shown that the meteoroid flux averages at 32.2 metric tons/day considering the largest object statistically expected to hit the Earth every day has a diameter of 0.5 m (Drolshagen et al., 2017). However, objects of such size in a hypervelocity entry (Hunt et al., 2004) and excitation temperatures around 4,400 K (Jenniskens, 2004) are expected to fully demise (Guttormsen et al., 2020). Further, a comprehensive analysis of historic meteorite surveys as to chemical composition points to a mean aluminum mass fraction of 1.2% (Schulz & Glassmeier, 2021). The TOA aluminum injection from micrometeoroids is 141.1 metric tons/year, and it is taken to be time-invariant. As for anthropogenic contributions, satellite-related objects reentering from LEO totaled 121.8 metric tons in 2016 (ESA, 2017) and 308.9 metric tons in 2022 (ESA, 2023). Concerning the future mega-constellations scenario, the worst-case estimation of Organski et al. (2020) is taken, with up to 3,200 metric tons of satellites reentering each year.

We then estimate an increase in TOA aluminum compounds (and excess ratio) originated from satellites, from 5.36 metric tons in 2016 (3.8% in excess of natural sources) to 41.7 metric tons in 2022 (excess of 29.5%). The future mega-constellations scenario of increased reentry rates would lead to 912.0 metric tons per year of TOA aluminum from satellites only (excess of 646%).

The long-term assessment next focuses on reentry byproducts. Note, however, that such analysis is solely performed for anthropogenic objects. Natural sources of aluminum such as micrometeoroids are originated from unbounded orbits and present high relative entry speeds. Therefore, no assumption can be made as to the fraction of aluminum from micrometeoroids that gets oxidized based in this MD simulation. Furthermore, and as previously

highlighted, up to 95% of the satellite's mass burns up upon reentry. For large satellite constellations, it was reported by major operators that their satellites' reduced mass and reentry trajectory will lead to a full burn-up during atmospheric reentry (OneWeb, 2016; SpaceX, 2020). As such, a survivability of 5% is assumed across the entire population of reentering satellites. This is then used to equate the mass fraction of aluminum that gets oxidized.

Based on the TOA influx of aluminum and the one-satellite aluminum oxide yield discussed above, we estimate an eight-fold increase in aluminum oxide compounds originated from satellites took place in the last couple of years, from 2.13 metric tons in 2016 to 16.6 metric tons in 2022. The future mega-constellations scenario of increased reentry rates would yield 362.7 metric tons per year of aluminum oxide compounds.

4. Summary and Conclusions

This paper presents the first atomic-scale MD simulation of the aluminum oxidation process for a small satellite during atmospheric reentry. The scenario appreciated is for a satellite originated in LEO and undergoing thermal ablation at the top of the mesosphere. Results are utilized to estimate the accumulation of reentry byproducts in the mesosphere, and the settling time of such byproducts until they reach the ozone layer. The atomic-scale simulation results are extrapolated using similarity parameters that support scalability.

MD simulation results show that the byproducts generated tend to rearrange into aluminum oxide clusters and aluminum clusters as the reaction takes place in an oxygen-deficient environment. As a result, aluminum oxide clusters are created after the impingement of oxygen into the original aluminum structure while large clusters of unoxidized aluminum may remain. Furthermore, we find that these reentry byproducts may take up to 30 years to settle from the top of the mesosphere into the stratospheric ozone layer. Upon reaching an altitude of about 40 km, aluminum oxides catalyze chlorine activation which promotes ozone depletion. This suggests that concentrations of aluminum oxide compounds may start increasing in the mesosphere well before reaching the stratospheric ozone layer. This would introduce a noticeable delay between the beginning of the injection process when orbiting bodies are decommissioned and the eventual ozone-depletion consequences in the stratosphere.

For a 250-kg satellite with a 30% aluminum mass fraction at reentry, we find that approximately 32% of the aluminum content gets oxidized, generating 29.8 kg of aluminum oxide clusters. Extrapolating this to the entire population of satellites reentering from LEO in 2022, we estimate that 41.7 metric tons of aluminum reentered the atmosphere, exceeding the natural level from micrometeoroids by 29.5%. Assuming the oxidized material scales linearly with reentered mass, we find that 16.6 metric tons of aluminum oxide compounds are generated from the aluminum influx of spacecraft debris to the mesosphere in 2022. Looking into the future by applying reentry forecasts considering the deployment of mega-constellations, the aluminum excess ratio at the top of the mesosphere can reach an yearly excess of more than 640% above natural levels, or over 360 metric tons of aluminum oxide clusters per year from satellites.

Due to their small size, the byproducts of spacecraft reentry can endure in the atmosphere and remain unnoticed until ozone concentration levels start decreasing. As reentry rates increase, it is crucial to further explore the concerns highlighted in this study. This paper only considered aluminum oxidation due to thermal ablation. The satellite angle of attack during reentry is taken to be constant, thus assuming a controlled reentry profile. Further, the atmospheric model does not account for diffusive or nucleation processes between byproducts. In the simulation, the molecular oxygen number density is taken to be constant due to the short duration of reentry and atomic oxygen is neglected. The MD model does not take into account all chemical species in aluminum alloys and in the air mixture due to the lack of interatomic potentials between such species. These will be addressed in future studies.

Data Availability Statement

The data on which this article is based are available in Ferreira et al. (2024).

Acknowledgments
This research is supported in part by the Future Investigators in NASA Earth and Space Science and Technology (FINESST) fellowship, NASA Grant 80NSSC22K1867. J.P.F. is also supported by a Fulbright Portugal Grant for Graduate Studies. K.N. is partially supported by NSF Grant OAC-2118061. The simulations were performed at the USC Center for Advanced Research Computing.

References

Anselmo, L., & Pardini, C. (2005). Computational methods for reentry trajectories and risk assessment. *Advances in Space Research*, *35*(7), 1343–1352. https://doi.org/10.1016/j.asr.2005.04.089

Beck, J., Holbrough, I., Schleutker, T., & Guelhan, A. (2019). Improved representation of destructive spacecraft re-entry from analysis of high enthalpy wind tunnel tests of spacecraft and equipment. *Acta Astronautica*, *164*, 287–296. https://doi.org/10.1016/j.actaastro.2019.07.033

Bekki, S., Beck, J., Lips, T., Merrifield, J., Spel, M., & Langener, T. (2021). Environmental impacts of atmospheric emissions from spacecraft re-entry demise. In *ESA clean space industrial days*. Retrieved from https://indico.esa.int/event/321/contributions/6403/attachments/4335/6538/esa-csid-21-bekki.pdf

Bianchi, S., Grassi, L., Benedetti, G., Giacone, R., Yamashita, H., Dahlmann, K., et al. (2021). Atmospheric re-entry assessment. In *ESA clean space industrial days*. Retrieved from https://indico.esa.int/event/321/contributions/6376/attachments/4334/6537/DESI_Bianchi_CleanSpaceIndustrialDays_ARA.pdf

Bonvoisin, B., Meisnar, M., Merrifield, J., Beck, J., Lips, T., Gülhan, A., et al. (2023). Demisability assessment of space materials. *CEAS Space Journal*, *15*, 213–235. https://doi.org/10.1007/s12567-022-00429-0

Brady, B., Fournier, E., Martin, L., & Cohen, R. (1994). Stratospheric ozone reactive chemicals generated by space launches worldwide (Aerospace Report No. TR-94(4231)-6). *The Aerospace Coorporation*. https://apps.dtic.mil/sti/pdfs/ADA289852.pdf

Ceplecha, Z., Borovička, J., Elford, W., ReVelle, D., Hawkes, R., Porubčan, V., & Šimek, M. (1998). Meteor phenomena and bodies. *Space Science Reviews*, *84*, 327–471. https://doi.org/10.1023/A:1005069928850

COESA. (1976). U.S. Standard Atmosphere 1976 (Tech. Rep. Nos. NOAA-S/T 76-1562, NASA-TM-X-74335). Committee on Extension to the Standard Atmosphere.

Cunningham, E. (1910). On the velocity of steady fall of spherical particles through fluid medium. *Proceedings of the Royal Society of London. Series A*, *83*(563), 357–365. https://doi.org/10.1098/rspa.1910.0024

Davies, C. (1945). Definitive equations for the fluid resistance of spheres. *Proceedings of the Physical Society*, *57*(4), 259–270. https://doi.org/10.1088/0959-5309/57/4/301

Drolshagen, G., Koschny, D., Drolshagen, S., Kretschmer, J., & Poppe, B. (2017). Mass accumulation of earth from interplanetary dust, meteoroids, asteroids and comets. *Planetary and Space Science*, *143*, 21–27. https://doi.org/10.1016/j.pss.2016.12.010

Eberhart, J., & Horner, S. (2010). Bond-energy and surface-energy calculations in metals. *Journal of Chemical Education*, *87*(6), 608–612. https://doi.org/10.1021/ed100189v

ESA. (2017). ESA's annual space environment report (Tech. Rep. No. GEN-DB-LOG-00208-OPS-GR). *ESA Space Debris Office*. Retrieved from https://www.sdo.esoc.esa.int/publications/Space_Environment_Report_I1R2_20170427.pdf

ESA. (2023). ESA's annual space environment report (Tech. Rep. No. GEN-DB-LOG-00288-OPS-SD). *ESA Space Debris Office*. Retrieved from https://www.sdo.esoc.esa.int/environment_report/Space_Environment_Report_latest.pdf

Falle, A., Wright, E., Boley, A., & Byers, M. (2023). One million (paper) satellites. *Science*, *382*(6667), 150–152. https://doi.org/10.1126/science.adi4639

FCC. (2021). Request for modification of the authorization for the SpaceX NGSO satellite system (Tech. Rep. No. FCC-21-48). *Federal Communications Commission*. Retrieved from https://www.fcc.gov/document/fcc-grants-spacexs-satellite-broadband-modification-application

FCC. (2022a). Request for orbital deployment and operating authority for the SpaceX Gen2 NGSO satellite system (Tech. Rep. No. FCC-22-91). Retrieved from https://www.fcc.gov/document/fcc-partially-grants-spacex-gen2-broadband-satellite-application

FCC. (2022b). Mitigation of orbital debris in the new space age (Tech. Rep. No. FCC-22-74). *Federal Communications Commission*. Retrieved from https://www.fcc.gov/document/fcc-adopts-new-5-year-rule-deorbiting-satellites-0

Ferreira, J. P., Huang, Z., Nomura, K., & Wang, J. (2024). Potential ozone depletion from satellite demise during atmospheric reentry in the era of mega-constellations [Dataset]. *Zenodo*. https://doi.org/10.5281/zenodo.10816330

Ferreira, J. P., Nomura, K., & Wang, J. (2023a). The byproducts of space debris upon atmospheric reentry and their polluting potential. In *2nd international orbital debris conference*. Retrieved from https://www.hou.usra.edu/meetings/orbitaldebris2023/pdf/6035.pdf

Ferreira, J. P., Nomura, K., & Wang, J. (2023b). Preliminary assessment of environmental impacts from the demise of reentering satellites in the upper atmosphere. In *AIAA ASCEND*. https://doi.org/10.2514/6.2023-4773

Guttormsen, G., Fletcher, A., & Oppenheim, M. (2020). Atomic-scale simulations of meteor ablation. *Journal of Geophysical Research: Space Physics*, *125*(9), e2020JA028229. https://doi.org/10.1029/2020JA028229

Hanning-Lee, M., Brady, B., Martin, L., & Syage, J. (1996). Ozone decomposition on alumina: Implications for solid rocket motor exhaust. *Geophysical Research Letters*, *23*(15), 1961–1964. https://doi.org/10.1029/96GL01808

Hong, S., & van Duin, A. (2015). Molecular dynamics simulations of the oxidation of aluminum nanoparticles using the reaxff reactive force field. *The Journal of Physical Chemistry C*, *119*(31), 17876–17886. https://doi.org/10.1021/acs.jpcc.5b04650

Huang, Z., Nomura, K., & Wang, J. (2021). Molecular dynamics simulations of water formation and retention by micrometeoroid impact on lunar surface. *Geophysical Research Letters*, *48*(15), e2021GL093509. https://doi.org/10.1029/2021GL093509

Huber, K., & Herzberg, G. (2013). Constants of diatomic molecules. In *Molecular spectra and molecular structure* (pp. 8–689). https://doi.org/10.1007/978-1-4757-0961-2

Hunt, S., Oppenheim, M., Close, S., Brown, P., McKeen, F., & Minardi, M. (2004). Determination of the meteoroid velocity distribution at the earth using high-gain radar. *Icarus*, *168*(1), 34–42. https://doi.org/10.1016/j.icarus.2003.08.006

Hunten, D., Turco, R., & Toon, O. (1980). Smoke and dust particles of meteoric origin in the mesosphere and stratosphere. *Journal of the Atmospheric Sciences*, *37*(6), 1342–1357. https://doi.org/10.1175/1520-0469(1980)037⟨1342:SADPOM⟩2.0.CO;2

IADC. (2021). IADC space debris mitigation guidelines (Tech. Rep. No. 1, Rev. 3). *Inter-Agency Space Debris Coordination Committee*. Retrieved from https://iadc-home.org/documents_public/file_down/id/5249

Jenniskens, P. (2004). Meteor induced chemistry, ablation products, and dust in the middle and upper atmosphere from optical spectroscopy of meteors. *Advances in Space Research*, *33*(9), 1444–1454. https://doi.org/10.1016/j.asr.2003.05.001

Jette, E., & Foote, F. (1935). Precision determination of lattice constants. *The Journal of Chemical Physics*, *3*(10), 605–616. https://doi.org/10.1063/1.1749562

Kärräng, P., Lips, T., & Soares, T. (2019). Demisability of critical spacecraft components during atmospheric re-entry. *Journal of Space Safety Engineering*, *6*(3), 181–187. https://doi.org/10.1016/j.jsse.2019.08.003

Knudsen, M., & Weber, S. (1911). Luftwiderstand gegen die langsame bewegung kleiner kugeln. *Annalen der Physik*, *341*(15), 981–994. https://doi.org/10.1002/andp.19113411506

Li, Y., Kalia, R., Nakano, A., & Vashishta, P. (2013). Size effect on the oxidation of aluminum nanoparticle: Multimillion-atom reactive molecular dynamics simulations. *Journal of Applied Physics*, *114*(13), 134312. https://doi.org/10.1063/1.4823984

Lips, T., Löhle, S., Marynowsky, T., Rees, D., Stenbeak-Nielsen, H., Beks, M., & Hatton, J. (2010). Assessment of the ATV-1 re-entry observation campaign for future re-entry missions. In *4th IAASS conference*. Retrieved from https://articles.adsabs.harvard.edu/pdf/2010ESASP.680E..47L

Löhle, S., Zander, F., Lemmens, S., & Krag, H. (2017). Airborne observations of re-entry break-up results and prospects. In *7th European conference on space debris*. Retrieved from https://conference.sdo.esoc.esa.int/proceedings/sdc7/paper/410/SDC7-paper410.pdf

Lohn, P., Wong, E., Molina, M., & Denison, R. (1994). *The impact of deorbiting space debris on stratospheric ozone (Tech. Rep. No. ADA414310)*. TRW Inc. Retrieved from https://apps.dtic.mil/sti/citations/ADA414310

Molina, M., Molina, L., Zhang, R., Meads, R., & Spencer, D. (1997). The reaction of $CLONO_2$ with HCL on aluminum oxide. *Geophysical Research Letters*, *24*(13), 1619–1622. https://doi.org/10.1029/97GL01560

Morrissey, L., Handrigan, S., Nakhla, S., & Rahnamoun, A. (2019). Erosion of spacecraft metals due to atomic oxygen: A molecular dynamics simulation. *Journal of Spacecraft and Rockets*, *56*(4), 1231–1236. https://doi.org/10.2514/1.A34414

Murphy, D., Abou-Ghanem, M., Cziczo, D., Froyd, K., Jacquot, J., Lawler, M., et al. (2023). Metals from spacecraft reentry in stratospheric aerosol particles. *Proceedings of the National Academy of Sciences of the United States of America*, *120*(43), e2313374120. https://doi.org/10.1073/pnas.2313374120

Nomura, K., Kalia, R., Nakano, A., Rajak, P., & Vashishta, P. (2020). RXMD: A scalable reactive molecular dynamics simulator for optimized time-to-solution. *SoftwareX*, *11*, 100389. https://doi.org/10.1016/j.softx.2019.100389

OneWeb. (2016). *Application for fixed satellite service by application for fixed satellite service by WorldVu Satellites Limited - orbital debris mitigation plan (Tech. Rep. No. SAT-LOI-20160428-00041/1158014)*. WorldVu Satellites Limited. Retrieved from https://fcc.report/IBFS/SAT-LOI-20160428-00041/1158014

Organski, L., Barber, B., Barkfelt, S., & Hobbs, M. (2020). Environmental impacts of satellites from launch to deorbit and the green new deal for the space enterprise. In *AGU fall meeting*. Retrieved from https://ui.adsabs.harvard.edu/abs/2020AGUFMGC0420004H

Pardini, C., & Anselmo, L. (2019). Uncontrolled re-entries of spacecraft and rocket bodies: A statistical overview over the last decade. *Journal of Space Safety Engineering*, *6*(1), 30–47. https://doi.org/10.1016/j.jsse.2019.02.001

Park, S., Laboulais, J., Leyland, P., & Mischler, S. (2021). Re-entry survival analysis and ground risk assessment of space debris considering by-products generation. *Acta Astronautica*, *179*, 604–618. https://doi.org/10.1016/j.actaastro.2020.09.034

Plane, J., Daly, S., Feng, W., Gerding, M., & Gómez Martín, J. (2021). Meteor-ablated aluminum in the mesosphere-lower thermosphere. *Journal of Geophysical Research: Space Physics*, *126*(2), e2020JA028792. https://doi.org/10.1029/2020JA028792

Rahman, A. (1964). Correlations in the motion of atoms in liquid argon. *Physics Reviews*, *136*(2A), A405–A411. https://doi.org/10.1103/PhysRev.136.A405

Randel, W., Stolarski, R., Cunnold, D., Logan, J., Newchurch, M., & Zawodny, J. (1999). Trends in the vertical distribution of ozone. *Science*, *285*(5434), 1689–1692. https://doi.org/10.1126/science.285.5434.1689

Ross, M., Ballenthin, J., Gosselin, R., Meads, R., Zittel, P., Benbrook, J., & Sheldon, W. (1997). In-situ measurement of Cl_2 and O_3 in a stratospheric solid rocket motor exhaust plume. *Geophysical Research Letters*, *24*(14), 1755–1758. https://doi.org/10.1029/97GL01592

Ross, M., Benbrook, J., Sheldon, W., Zittel, P., & McKenzie, D. (1997). Observation of stratospheric ozone depletion in rocket exhaust plumes. *Nature*, *390*(6655), 62–64. https://doi.org/10.1038/36318

Schulz, L., & Glassmeier, K. (2021). On the anthropogenic and natural injection of matter into earth's atmosphere. *Advances in Space Research*, *67*(3), 1002–1025. https://doi.org/10.1016/j.asr.2020.10.036

Scott, T., Dieudonne, W., & Spel, M. (2004). MISTRAL: CONUS Début flow field and heat transfer calculations. In *34th AIAA fluid dynamics conference and exhibit*. https://doi.org/10.2514/6.2004-2423

Skinner, L., Barnes, A., Salmon, P., Hennet, L., Fischer, H., Benmore, C., et al. (2013). Joint diffraction and modeling approach to the structure of liquid alumina. *Physical Review B: Condensed Matter and Materials Physics*, *87*(2), 024201. https://doi.org/10.1103/PhysRevB.87.024201

SpaceX. (2020). *Application for fixed satellite service by Space Exploration Holdings, LLC – Attachment A (Tech. Rep. No. SAT-MOD-20200417-00037)*. Space Exploration Holdings LLC. Retrieved from https://fcc.report/IBFS/SAT-MOD-20200417-00037/2274316

Stukowski, A. (2009). Visualization and analysis of atomistic simulation data with OVITO–the open visualization tool. *Modelling and Simulation in Materials Science and Engineering*, *18*(1), 015012. https://doi.org/10.1088/0965-0393/18/1/015012

Thomas, D., & Charvet, A. (2017). An introduction to aerosols. In *Aerosol filtration* (pp. 1–30). https://doi.org/10.1016/B978-1-78548-215-1.50001-9

Van Duin, A., Dasgupta, S., Lorant, F., & Goddard, W. (2001). Reaxff: A reactive force field for hydrocarbons. *The Journal of Physical Chemistry A*, *105*(41), 9396–9409. https://doi.org/10.1021/jp004368u

Vashishta, P., Kalia, R., & Nakano, A. (2006). Multimillion atom simulations of dynamics of oxidation of an aluminum nanoparticle and nanoindentation on ceramics. *The Journal of Physical Chemistry B*, *110*(8), 3727–3733. https://doi.org/10.1021/jp0556153

Waswa, P., & Hoffman, J. (2012). Illustrative NASA low earth orbit spacecraft subsystems design-for-demise trade-offs, analyses and limitations. *International Journal of Design Engineering*, *5*(1), 21–40. https://doi.org/10.1504/IJDE.2012.050280

Weidmann, D. (2021). Atmospheric trace gas measurements using laser heterodyne spectroscopy. In *Advances in spectroscopic monitoring of the atmosphere* (pp. 159–223). https://doi.org/10.1016/B978-0-12-815014-6.00005-1

Wertz, J., Everett, D., & Puschell, J. (2011). *Space mission engineering: The new SMAD* (p. 674).

Winter, M. (2014). Airborne observation of re-entries - Lessons learned and future perspectives (invited). In *19th AIAA international space planes and hypersonic systems and technologies conference*. https://doi.org/10.2514/6.2014-2806

Zhang, C., Kalia, R., Nakano, A., Vashishta, P., & Branicio, P. (2008). Deformation mechanisms and damage in α-alumina under hypervelocity impact loading. *Journal of Applied Physics*, *103*(8), 083508. https://doi.org/10.1063/1.2891797

Zolensky, M., McKay, D., & Kaczor, L. (1989). A tenfold increase in the abundance of large solid particles in the stratosphere, as measured over the period 1976–1984. *Journal of Geophysical Research*, *94*(D1), 1047–1056. https://doi.org/10.1029/JD094iD01p01047